A&A 479, 75–82 (2008)
DOI: 10.1051/0004-6361:20078018

Astronomy & Astrophysics

^{12}CO 4–3 and [CI] 1–0 at the centers of NGC 4945 and Circinus

M. Hitschfeld[1], M. Aravena[3], C. Kramer[1], F. Bertoldi[3], J. Stutzki[1], F. Bensch[3], L. Bronfman[4], M. Cubick[1], M. Fujishita[5], Y. Fukui[5], U. U. Graf[1], N. Honingh[1], S. Ito[5], H. Jakob[1], K. Jacobs[1], U. Klein[3], B.-C. Koo[6], J. May[4], M. Miller[1], Y. Miyamoto[5], N. Mizuno[5], T. Onishi[5], Y.-S. Park[6], J. L. Pineda[3], D. Rabanus[1], M. Röllig[3], H. Sasago[5], R. Schieder[1], R. Simon[1], K. Sun[1], N. Volgenau[1], H. Yamamoto[5], and Y. Yonekura[2]

[1] KOSMA, I. Physikalisches Institut, Universität zu Köln, Zülpicher Straße 77, 50937 Köln, Germany
e-mail: hitschfeld@ph1.uni-koeln.de
[2] Department of Physical Science, Osaka Prefecture University, Osaka 599-8531, Japan
[3] Argelander-Institut für Astronomie, Auf dem Hügel 71, 53121 Bonn, Germany
[4] Departamento de Astronomía, Universidad de Chile, Casilla 36-D, Santiago, Chile
[5] Department of Astrophysics, Nagoya University, Chikusa-ku, Nagoya 464-8602, Japan
[6] Seoul National University, Seoul 151-742, Korea

Received 5 June 2007 / Accepted 7 November 2007

ABSTRACT

Context. Studying molecular gas in the central regions of the star burst galaxies NGC 4945 and Circinus enables us to characterize the physical conditions and compare them to previous local and high-z studies.
Aims. We estimate temperature, molecular density and column densities of CO and atomic carbon. Using model predictions we give a range of estimated CO/C abundance ratios.
Methods. Using the new NANTEN2 4 m sub-millimeter telescope in Pampa La Bola, Chile, we observed for the first time CO 4–3 and [C I] $^3P_1$–$^3P_0$ at the centers of both galaxies at linear scale of 682 pc and 732 pc respectively. We compute the cooling curves of ^{12}CO and ^{13}CO using radiative transfer models and estimate the physical conditions of CO and [CI].
Results. The centers of NGC 4945 and Circinus are very [C I] bright objects, exhibiting [C I] $^3P_1$–$^3P_0$ luminosities of 91 and 67 K km s^{-1} kpc^2, respectively. The [C I] $^3P_1$–$^3P_0$/CO 4–3 ratio of integrated intensities are large at 1.2 in NGC 4945 and 2.8 in Circinus. Combining previous CO J = 1–0, 2–1 and 3–2 and ^{13}CO J = 1–0, 2–1 studies with our new observations, the radiative transfer calculations give a range of densities, $n(H_2) = 10^3$–3×10^4 cm^{-3}, and a wide range of kinetic temperatures, T_{kin} = 20–100 K, depending on the density. To discuss the degeneracy in density and temperature, we study two representative solutions. In both galaxies the estimated total [CI] cooling intensity is stronger by factors of ∼1–3 compared to the total CO cooling intensity. The CO/C abundance ratios are 0.2–2, similar to values found in Galactic translucent clouds.
Conclusions. Our new observations enable us to further constrain the excitation conditions and estimate the line emission of higher-J CO- and the upper [CI]-lines. For the first time we give estimates for the CO/C abundance ratio in the center regions of these galaxies. Future CO J = 7–6 and [CI] 2–1 observations will be important to resolve the ambiguity in the physical conditions and confirm the model predictions.

Key words. galaxies: starburst – galaxies: nuclei – galaxies: ISM – galaxies: active – galaxies: individual: NGC 4945 – galaxies: individual: Circinus

1. Introduction

The spiral galaxies NGC 4945 and Circinus at distances of ∼3.7 and ∼4 Mpc belong to the nearest and infrared brightest galaxies in the sky. Their strong central star burst activity is fed by large amounts of molecular material and this has been studied extensively at millimeter wavelengths (e.g. Curran et al. 2001a; Wang et al. 2004). However, sub-millimeter observations are largely missing. The important rotational transitions of CO with $J \geq 4$ and the fine structure transitions of atomic carbon have not yet been observed. These transitions often contribute significantly to the thermal budget of the interstellar gas in galactic nuclei and are therefore important tracers of the physical conditions of the warm and dense gas.

Emission of CO, [C I] (and [C II]) traces the bulk of carbon bearing species in molecular clouds that play an important role in their chemical network. The CO 4–3 transition in particular is a sensitive diagnostic of the dense and warm gas while the CO 1–0 transition traces the total molecular mass. The [C I] $^3P_1$–$^3P_0$ (henceforth 1–0) line has, to date, been detected in about 30 galactic nuclei (Gerin & Phillips 2000; Israel & Baas 2002; Israel 2005) and appears to trace the surface regions of clumps illuminated by the FUV field of newborn, massive stars (e.g. Kramer et al. 2004, 2005). The use of CI as an accurate tracer of the cloud mass has been discussed with controversy (Frerking et al. 1989; Papadopoulos & Greve 2004; Mookerjea et al. 2006).

The strong cooling emission is balanced by equally strong heating caused by the vigorous star formation activity in the galaxy centers. The variation of CO cooling intensities with rotational number, i.e. the peak of the CO cooling curve, reflects the star forming activity (Bayet et al. 2006) and, possibly, also the underlying heating mechanisms. Several mechanisms have been proposed to explain the heating of the ISM in galactic nuclei and it is currently rather unclear which of these dominates in individual sources (e.g. Wang et al. 2004). Heating by X-rays from the active galactic nuclei (AGN) may lead to strongly

enhanced intensities of high-J CO transitions (Meijerink et al. 2007), possibly allowing one to discriminate this heating mechanism from e.g. stellar ultraviolet heating via photon dominated regions (PDRs) (e.g. Bayet et al. 2006). The greatly enhanced supernova rate by several orders of magnitude relative to the solar system value leads to an enhanced cosmic ray flux, providing another source of gas heating in the centers (Farquhar et al. 1994; Bradford et al. 2003). Another mechanism for heating is provided by shocks. The most important, large-scale shocks are produced by density wave instabilities which induce gravitational torques (in spiral arms and/or bars) and make the gas fall into the nucleus (Usero et al. 2006). A non-negligible contribution is also given by shocks produced by supernovae explosions. On smaller scales, bipolar outflows from young stellar objecs (YSO) can also contribute to this heating, although to a lesser extent (e.g. García-Burillo et al. 2001).

1.1. NGC 4945

NGC 4945, a member of the Centaurus group of galaxies, is seen nearly edge-on (Table 1) with an optical diameter of ∼20′ (de Vaucouleurs et al. 1991). H I kinematics indicate a galaxy mass of $1.4 \times 10^{11}\,M_\odot$ within a radius of 6.3′ with molecular and neutral atomic gas contributing ∼2% respectively (Ott et al. 2001).

With a dynamical mass of $\sim 3 \times 10^9\,M_\odot$ in the central 600 pc (Mauersberger et al. 1996), it is one of the strongest IRAS point sources with almost all the far infrared luminosity coming from the nucleus (Brock et al. 1988). Observations of the X-ray spectrum are consistent with a Seyfert nucleus (Iwasawa et al. 1993), and further analysis of optical imaging and infrared spectra (Moorwood & Oliva 1994) suggests that this object is in a late stage on the transition from starburst to a Seyfert galaxy. Its nucleus was the first source in which a powerful H_2O mega maser was detected (Dos Santos & Lépine 1979).

Studies in H I (Ables et al. 1987) and low-J CO transitions (Whiteoak et al. 1990; Dahlem et al. 1993; Ott 1995; Mauersberger et al. 1996) suggest the presence of a face-on circumnuclear molecular ring. Millimeter molecular multiple transition studies (Wang et al. 2004; Cunningham & Whiteoak 2005) are consistent with this result. The bright infrared and radio emission in the nucleus (Ghosh et al. 1992), and the evidence that large amounts of gas seem to coexist in the central 30″ (Henkel et al. 1994) make it particularly suited for studying the high density environment in the center of this galaxy.

1.2. Circinus

The nearby starburst spiral Circinus has a small optical angular diameter of ∼7′ compared to its hydrogen diameter $D_{\rm H} = 36'$ defined by the 1×10^{20} atoms cm^{-2} contour in Freeman et al. (1977).

Circinus has a dynamical mass of $\sim 3 \times 10^9\,M_\odot$ within the inner 560 pc (Curran et al. 1998) matching the value obtained for NGC 4945. Large amounts of molecular gas have been found by studies of low-J CO observations (Johansson et al. 1991; Aalto et al. 1995; Elmouttie et al. 1998; Curran et al. 1998) including $C^{17}O$, $C^{18}O$ and HCN (Curran et al. 2001a). The strong H_2O maser emission found (Gardner & Whiteoak 1982) traces a thin accretion disk of 0.8 pc radius, with a significant population of masers lying away from this disk, possibly in an outflow (Greenhill et al. 1998). Its obscured nucleus is classified as an X-ray Compton thick Seyfert 2. It shows a circumnuclear star burst on scales of 100−200 pc (Maiolino et al. 1998) with a complex structure of H II as seen in Hubble Space Telescope (HST) Hα images (Wilson et al. 2000). Adaptive optics studies find there has been a recent star burst (∼100 Myr old) in the central 8 pc accounting for 2% of the total luminosity (Mueller Sánchez et al. 2006). The strong FIR emission, the large molecular gas reservoir, the existence of a molecular ring associated with star burst activity (Curran et al. 1998) and the similarity with NGC 4945 make them ideal objects for comparative studies of the dense and warm ISM in their nuclei.

Table 1. Basic properties of Circinus, NGC 4945 and NGC 253.

	Circinus	NGC 4945	NGC 253
RA(2000)	14:13:09.9	13:05:27.4	00:47:33.1
Dec(2000)	–65:20:21	–49:28:05	–25:17:18
Type	SA(s)b[a]	SB(s)cd[a]	SAB(s)c[a]
Distance [Mpc]	4.0[d]	3.7[b]	3.5[e]
38″ correspond to	732 pc	682 pc	646 pc
LSR velocity [km s^{-1}]	434	555	243
Inclination [deg]	65[c]	78[b]	78[a]
$L_{\rm IR}$ [$10^{10}\,L_\odot$]	1.41[g]	1.39[g]	2.67[g]
S_{100}[Jy]	3.16×10^2	6.86×10^2	10.4×10^2

$L_{\rm IR}$ is the total mid and far infrared luminosity calculated from the flux densities at 12 μm, 25 μm, 60 μm, 100 μm listed in the IRAS point source catalogue (Lonsdale & Helou 1985) using the formulae given in Table 1 of Sanders & Mirabel (1996) and the distances listed below. References: [a] RC3 catalogue of de Vaucouleurs et al. (1991), [b] Mauersberger et al. (1996), [c] Freeman et al. (1977), [d] Curran et al. (1998), [e] Rekola et al. (2005), [f] Curran et al. (2001b), [g] Fullmer & Londsdale (1989).

2. Observations

We used the new NANTEN2 sub-millimeter telescope (e.g. Kramer et al. 2007) on Pampa la Bola at an elevation of 4900 m together with a dual channel 490/810 GHz receiver (operated jointly by the Nagoya University radioastronomy group and the KOSMA group from Universität zu Köln) to observe the centers of NGC 4945, Circinus, and NGC 253 (Table 1) in CO 4–3 and [C I] 1–0. The observations were performed from September to October 2006 using the position-switch mode with 20 s On- and 20 s Off-time. In October 2007 we reobserved ^{12}CO 4–3 in the centers of NGC4945 and Circinus with the newly available chopping tertiary in double beam-switch mode yielding significantly improved baselines and removing atmospheric features in the spectra. In NGC 4945 the total integration times ON-source are 17 min and 10 min for ^{12}CO 4–3 and [C I] 1–0 respectively and in Circinus integration times ON-source are 10 min and 34 min for ^{12}CO 4–3 and [C I] 1–0 respectively at source elevations of 40−60°. The relative calibration uncertainty derived from repeated pointings on the nuclei is about 15%.

Position-switching was conducted by moving the telescope 10′ in azimuth, i.e. out of the galaxy. Using double beam-switch (dbs) mode, the chopper throw is fixed at 162″ in azimuth with a chopping frequency of 1 Hz. Typical double-sideband receiver temperatures of the dual-channel 460/810 GHz receiver were ∼250 K at 460 GHz and 492 GHz. The system temperature varied between ∼850 and ∼1200 K. As backends we used two acusto optical spectrometers (AOS) with a bandwidth of 1 GHz and a channel resolution of 0.37 km s^{-1} at 460 GHz and 0.21 km s^{-1} at 806 GHz. The pointing was regularly checked and pointing accuracy was stable with corrections of ∼10″. The

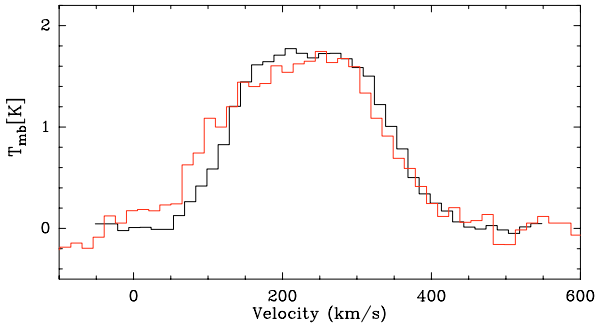

Fig. 1. Observed ^{12}CO 4–3 line emission in NGC 253 from APEX (black line) and NANTEN2 (red line). We attribute small but systematic deviations of peak temperatures in the blue wing of the ^{12}CO 4–3 line to small pointing variations.

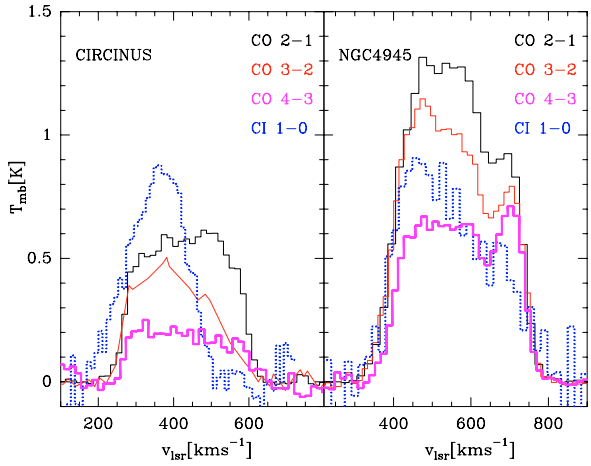

Fig. 2. CO 4–3 and [C I] 1–0 spectra of Circinus and NGC 4945 obtained with the NANTEN2 telescope together with low-J CO observations by Curran et al. (2001a, 1998); Mauersberger et al. (1996). All data are at 38″ resolution, only the CO 3–2 spectrum of Circinus is at 15″ resolution. The small amount of excess emission in the blue wing of the [C I] 1–0 line in Circinus maybe caused by small pointing variations in the eastern direction as emission in lower-J CO lines extends to this region and velocities (Curran et al. 1998).

half power beam width (HPBW) at 460 GHz and 492 GHz is 38″ with a beam efficiency $B_{\rm eff}$ = 0.50 and a forward efficiency $F_{\rm eff}$ = 0.86 (Simon et al. 2007). The calibrated data on $T_{\rm A}^*$-scale were converted to $T_{\rm mb}$ by multiplying by the ratio $F_{\rm eff}/B_{\rm eff}$. The standard calibration procedure derives the atmospheric transmission (averaged over the bandpass) from the observed difference spectrum of hot load and blank sky, the latter taken at a reference position. Next, the model atmosphere `atm` is used to derive the atmospheric opacity taking into account the sideband imbalance. This is an important correction, especially when observing the CO 4–3 and [CI] 1–0 lines. This pipeline produces the standard spectra on the antenna temperature scale (T_A^*). In addition, we removed baselines up to first order.

The 810 GHz channel was not used for these observations due to insufficient baseline stability.

All data presented in this paper are on the $T_{\rm mb}$ scale.

2.1. ^{12}CO 4–3 in NGC 253

To check the NANTEN2 calibration scheme, we retrieved the ^{12}CO 4–3 map of NGC 253 taken at APEX (Güsten et al. 2006) and smoothed it to the NANTEN2 HPBW of 38″ using a Gaussian kernel. The resulting spectra at the center position are shown in Fig. 1. Line temperatures and shapes show very good agreement.

3. Spectra of CO 4–3 and [C I] 1–0

Figure 2 shows the ^{12}CO 4–3 and [C I] 1–0 spectra of NGC 4945 and Circinus obtained with the NANTEN2 telescope. CO 4–3 spectra peak at 700 mK in NGC 4945 and 250 mK in Circinus. Outside the velocity ranges of 350–800 km s^{-1} and 200–600 km s^{-1} respectively, the baseline rms values are 11 mK and 25 mK, respectively, at the velocity resolution of 15 km s^{-1}. [C I] 1–0 spectra peak at 900 mK in both galaxies while the rms values are 110 mK and 140 mK, respectively. The [C I] 1–0 area-integrated luminosities are 91 K km s^{-1} kpc^2 and 67 K km s^{-1} kpc^2 in NGC 4945 and Circinus.

Curran et al. (2001a, 1998) and Mauersberger et al. (1996) mapped the low-J 2–1, and 3–2 transitions of CO in the centers of both galaxies with SEST. We smoothed these data to the resolution of the NANTEN2 data, i.e. to 38″. Only the ^{12}CO 3–2 spectrum in Circinus is shown at its original resolution of 15″ because a map of the central region could not be retrieved. Calibration of the CO 3–2 spectrum in NGC 4945 was confirmed recently at APEX (Risacher et al. 2006). The ^{12}CO 1–0, ^{13}CO 1–0 and ^{13}CO 2–1 spectra of the central region of NGC 4945 and Circinus are presented in Curran et al. (2001a). We list integrated intensities in Table 2.

Table 2. Observed line intensities in Circinus and NGC 4945.

line transition	Circinus $I_{\rm int}$ [K km s^{-1}]	NGC 4945 $I_{\rm int}$ [K km s^{-1}]	*FWHM* [″]
CO 1–0[a]	180	510	45
CO 2–1[a]	177	390	38
CO 3–2[b]	–	330	38
CO 3–2[b]	230	–	15
CO 4–3	58	212	38
^{13}CO 1–0[a]	12	30	45
^{13}CO 2–1[a]	19	45	38
[CI] 1–0	163	248	38

Calibration uncertainties are estimated to be 15%. The spectra in Fig. 2 and the integrated intensities correspond to the listed angular resolution (FWHM). References: [a]Curran et al. (2001a), [b] Mauersberger et al. (1996).

NGC 4945 shows broad emission between 350 and 800 km s^{-1}. The CO 4–3 line shape resembles the line shapes of 1–0 and 2–1. The line shape of [C I] 1–0 is similar to that of the CO transitions with a slighlty higher peak temperature than CO 4–3.

In CO 1–0 and 2–1, Circinus shows broad emission between 200 and about 600 km s^{-1}. The velocity component at ~550 km s^{-1} becomes weaker with rising rotational number. Emission of [C I] 1–0 is restricted to 200 and ~500 km s^{-1} only. In Circinus, the [C I] peak temperature is a factor ~3 stronger than CO 4–3.

4. Physical conditions

4.1. LTE

In the optically thin limit, the integrated intensities of [C I] and ^{13}CO listed in Table 2 are proportional to the total column densities. LTE column densities of carbon are rather

independent of the assumed excitation temperatures (e.g. Frerking et al. 1989). We find $N_C = 3.4–3.9 \times 10^{18}$ cm^{-2} in NGC 4945 and $N_C = 2.2–2.5 \times 10^{18}$ cm^{-2} in Circinus for a temperature range of $T_{ex} = 20–150$ K.

We used the ^{13}CO $J = 1–0$ and $J = 2–1$ integrated intensities to derive total CO column densities, assuming LTE, optically thin ^{13}CO emission, a CO/^{13}CO abundance ratio of 40 (Curran et al. 2001a), and $T_{ex} = 20$ K. We find a total CO column density of $N_{CO} = 1.0–1.7 \times 10^{18}$ cm^{-2} and $N_{CO} = 4.1–6.7 \times 10^{17}$ cm^{-2} in NGC 4945 and Circinus respectively depending on which transition is used, 1–0 or 2–1. Varying the temperature to $T_{ex} = 150$ K the column density of CO slightly increases up to $N_{CO} = 3.2 \times 10^{18}$ cm^{-2} and $N_{CO} = 1.4 \times 10^{18}$ cm^{-2} for NGC 4945 and Circinus.

Another method uses the Galactic CO 1–0 to H_2 conversion factor $X_{MW} = 2.3 \times 10^{20}$ cm^{-2} (K km s^{-1})$^{-1}$ (Strong et al. 1988; Strong & Mattox 1996) and the canonical CO to H_2 abundance of 8.5×10^{-5} (Frerking et al. 1982) to derive $N_{CO} = 3.5 \times 10^{18}$ cm^{-2} for Circinus, i.e. a factor of ∼10 larger than the LTE estimate indicating that the X-factor is only 1/10 Galactic. As the abundance of CO maybe different in NGC 4945 and Circinus this result has to be taken with caution.

For NGC 4945 Wang et al. (2004) derive an X-factor 7 times smaller than the Galactic value, which leads to $N_{CO} = 1.4 \times 10^{18}$ cm^{-2}, in good agreement with the LTE approximation from ^{13}CO. The LTE column density derived from ^{13}CO in Circinus also indicates an X-factor around 10 times smaller than the Galactic value.

The CO/C abundance ratio is 0.29–0.50 in NGC 4945 and 0.19–0.27 in Circinus using the LTE column densities.

4.2. Radiative transfer analysis of CO and ^{13}CO

We modeled the ^{12}CO and ^{13}CO emission lines using an escape probability radiative transfer model for spherical clumps (Stutzki & Winnewisser 1985) using the CO collision rates of Schinke et al. (1985). This non-LTE model assumes a uniform density and temperature in a homogenous clump. The physical parameters kinetic temperature T_{kin}, molecular density $n(H_2)$, and column density N_{CO} determine the excitation conditions in this model (Table 3).

In NGC 4945 and Circinus, we used the ratios of the observed integrated intensities of CO 1–0 to 4–3 and the ^{13}CO 1–0 and 2–1 transitions (Curran et al. 2001a) to obtain column densities, density and kinetic temperature, assuming a constant ^{12}CO/^{13}CO abundance ratio. We used an abundance ratio of 40 in both sources in accordance with Curran et al. (2001a). The escape probility code uses an internal clump line width Δv_{mod} which hardly effects the outcome of the model in the reasonable range of 1–20 km s^{-1}.

In a simultaneous fit a χ^2-fitting routine then compared the J line ratios of the model output R^j_{mod} to the ratios of the observed integrated intensities R^j_{obs} and determined the model with the minimal χ^2. We compute the normalized χ^2 with the degrees of freedom $d = J - p$ and J being the number of independent ratios and p the number of parameters, in our case T_{kin}, $n(H_2)$ and N_{CO}, to be determined:

$$\chi^2 = \frac{1}{d} \sum_{j=1}^{J} (R^j_{mod} - R^j_{obs})/\sigma_j. \quad (1)$$

The errors σ_j due to calibration uncertainties are estimated to be 20%.

Table 3. Escape probability model results with two representative solutions for each source.

	Circinus		NGC 4945	
χ^2	2.0	9.6	4.8	12.4
$n(H_2)_{loc}$ [cm^{-3}]	10^4	10^3	3×10^4	10^3
T_{kin} [K]	20	100	20	100
N_{CO} [10^{16} cm^{-2}]	35	50	76	63
N_C [10^{16} cm^{-2}]	230	30	330	98
N_{H_2} [10^{20} cm^{-2}]	37	46.5	89	74
M [10^6 $M_\odot$]	630	792	1385	1114
Δv_{mod} [km s^{-1}]	5	5	10	10
Δv_{obs} [km s^{-1}]	186	186	188	188
N_{cl}	50	38	35	40
ϕ_A	2.0	6.3	1.5	4.0
^{12}CO/^{13}CO abundance ratio	40	40	40	40
CO/C abundance ratio	0.15	1.67	0.23	0.64
[C I] cooling intensity	4.1	7.88	7.2	11.8
CO cooling intensity	2.1	2.8	6.6	5.7
[C I] /CO cooling intensity ratio	2.0	2.8	1.1	2.1

N_{CO} and N_{H_2} denote the total beam averaged column density of CO and H_2, i.e. local clump column densities weighted by the total area filling factor ϕ_A. M denotes the total mass. N_{cl} is the number of clumps in the beam, Δv_{mod} is the modeled velocity width and ϕ_A is the total filling factor to convert from modeled to observed intensities. The total cooling intensities are given in units of 10^{-5} erg s^{-1} cm^{-2} sr^{-1}.

In Circinus the ^{12}CO 3–2 line is missing, leaving one degree of freedom compared to two in NGC 4945.

T_{kin} and $n(H_2)$ are determined with this step. To compare the modeled integrated intensities I_{mod} to the absolute observed intensities I_{obs} we have to account for the velocity filling, due to the velocity width Δv_{mod} of an individual clump to the width of the galaxy spectrum Δv_{obs} and the beam dilution, due to the size of the modeled clump A_{cl} compared to the beam area A_{beam}.

The large velocity width of the observed spectra implies several clumps in the beam $N_{cl} = n\,\Delta v_{obs}/\Delta v_{mod}$ with $n \geq 1$ (Table 3). The beam dilution is determined by the fraction of modeled clump area to the beam size which we express in terms of an area filling factor per clump $\phi_{A,cl} = A_{cl}/A_{beam}$. The total area filling factor is $\phi_A = N_{cl}\,\phi_{A,cl}$. The size of the clump with radius R, $A_{cl} = \pi R^2$, can be inferred via the mass M and density $n(H_2)$ of the clump: $R = (3/(4\pi)M/n)^{(1/3)}$. In summary, the modeled intensities of the individual clumps I_{mod} are converted to the intensities of a clump ensemble I_{ens} which can then be compared with the observed intensities:

$$I_{ens} = I_{mod} \times N_{cl} \times \phi_{A,cl} = I_{mod} \times \phi_A. \quad (2)$$

4.2.1. NGC 4945

Figure 3b shows the observed intensities of CO, ^{13}CO, and [C I] together with two representative solutions of the radiative transfer calculations (see also Table 3).

CO. Fitting the CO and ^{13}CO lines, we find a degeneracy in the $n(H_2) - T_{kin}$ plane of the solutions for a rather constant pressure $n(H_2) \times T_{kin} \sim 10^5$ Kcm^{-3}. The best fits are achieved for a ^{12}CO/^{13}CO abundance ratio of 40, similar to the value found by Curran et al. (2001a). Low χ^2-values (see Table 3) constrain the densities to $n(H_2) = 10^3–10^5$ cm^{-3} and temperatures to a wide range of $T_{kin} = 20–180$ K with higher temperature solutions corresponding to lower densities. The best fitting solution

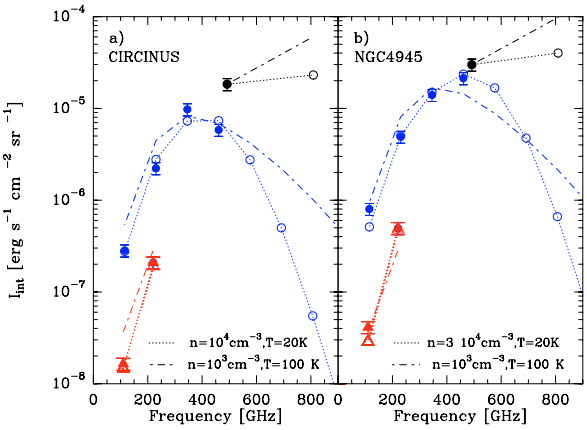

Fig. 3. Radiative transfer modeling results and observations: filled blue points show the observed CO and blue circles the modeled CO. The dotted line indicates the best fit solution. Filled red triangles show the observed ^{13}CO and red triangles the modeled ^{13}CO. Dash-dotted lines show a higher temperature solution. Filled black points are the observed [CI] integrated intensities and black circles the predicted [CI] integrated intensities.

is $n(H_2) = 3 \times 10^4$ cm^{-3} and $T_{kin} = 20$ K. However, this solution is not significantly better than e.g. $n(H_2) = 10^3$ cm^{-3} and $T_{kin} = 100$ K (Fig. 3b, Table 3).

The fitted column density N_{CO} agrees with the LTE approximation for the CO-column density within a factor of 2–3.

The peak of the modeled CO cooling curve at $J = 4$ contains 35.6% of the total ^{12}CO cooling intensity of 6.6×10^{-5} erg s^{-1} cm^{-2} sr^{-1} computed by summing the cooling intensity of the ^{12}CO transitions from $J = 1$ to 20 for the $T_{kin} = 20$ K solution.

We use the radiative transfer model to predict the ^{12}CO 7–6 intensity. It is rather weak, depending strongly on T_{kin}. It varies from 1.3 K km s^{-1} for the $T_{kin} = 20$ K solution to 4.1 K km s^{-1} for the $T_{kin} = 100$ K fit.

Curran et al. (2001a) find in this source $n(H_2) = 3 \times 10^3$ cm^{-3} and $T_{kin} = 100$ K from ^{12}CO observations of the 3 lowest transitions and ^{13}CO data of the two lowest transitions. In their multi-transition study Wang et al. (2004) estimate a density of $n(H_2) = 10^3$ cm^{-3} for an assumed temperature $T_{kin} = 50$ K from CO transitions up to $J = 3$. In contrast, the observed CN and CH_3OH lines indicate local densities around 10^4 cm^{-3}. The solutions for CO and ^{13}CO found in the literature are in good agreement with our parameter space of solutions showing that the additional CO 4–3 line does not help significantly to improve the fits.

Atomic carbon. Assuming the same density, kinetic temperature, velocity filling, and beam dilution for carbon as for CO, we use the observed [C I] intensity and the radiative transfer model to estimate the carbon column density and hence the CO/C abundance ratio. The CO/C abundance ratio varies between 0.23 and 0.64 for the two solutions listed in Table 3. The corresponding carbon column densities are $N_C = 3.3 \times 10^{18}$ cm^{-2} and $N_C = 9.8 \times 10^{17}$ cm^{-2} for the high and the low density solution, respectivly. The column density for the latter solution is a factor of 3 lower compared to the LTE carbon column density. The assumption of optically thin emission in the LTE might be overestimating the column density compared to the escape probability modelling. We also use the model to predict the [C I] 2–1 intensity. It is 16 K km s^{-1} for the $T_{kin} = 20$ K/$n(H_2) = 3 \times 10^4$ cm^{-3} solution. However, this result critically depends on the kinetic temperature. The $T_{kin} = 100$ K/$n(H_2) = 10^3$ cm^{-3} solution yields 182 K km s^{-1}. Also, the [C I] 2–1/[C I] 1–0 line ratios change from 0.07 to 0.75, depending on the solution. This shows that the high-lying transitions can be used to break the degeneracy.

The total cooling intensity of both [C I] lines is listed in Table 3 for both presented solutions. The cooling intensity of the two [C I] lines is thus of the order of the total cooling intensity of CO with the C/CO cooling intensity ratio varying between 1.1–2.1 for the discussed solutions.

4.2.2. Circinus

CO. The modeled CO cooling curves are shown in Fig. 3a and the fit results are summarized in Table 3. The CO line ratios are given for a $\Delta v_{mod} = 5$ km s^{-1} so there are about 40 clouds in the beam to account for the observed velocity width of $\Delta v_{obs} = 186$ km s^{-1}. The assumed ^{12}CO/^{13}CO abundance ratio of 40 is slightly lower than the values of ~60, found by Curran et al. (2001a).

Good fits corresponding to low χ^2 (see Table 3) can be found for densities of $n(H_2) = 10^3$–$10^{4.5}$ cm^{-3} and a large range of temperatures of $T_{kin} = 20$–160 K while the product of $n(H_2) \times T_{kin}$ stays approximately constant at $\sim 10^5$ Kcm^{-3}. Again, a number of solutions provide consistent CO cooling curves.

The lowest χ^2 is obtained for $n(H_2) = 10^4$ cm^{-3}, $T_{kin} = 20$ K and a column density of $N_{CO} = 3.5 \times 10^{17}$ cm^{-2} assuming 50 modeled clumps in the beam. The column density N_{CO} is well determined showing a steep gradient of χ^2-values for varying densities and temperatures. This is in reasonable agreement with the LTE-approximation from ^{13}CO. A second solution at $n = 10^3$ cm^{-3} and $T_{kin} = 100$ K also lies within the 1σ-contour of the χ^2 distribution (cf. Fig. 3 and Table 3).

The results agree well with the solutions found by Curran et al. (2001a). They find $T_{kin} = 50$–80 K and $n(H_2) = 2 \times 10^3$ cm^{-3} from observations of the 3 lowest ^{12}CO transitions and the 2 lowest ^{13}CO transitions.

The modeled CO cooling curve peaks at $J = 4$ containing 35% of the total ^{12}CO cooling intensity of 2.1×10^{-5} erg s^{-1} cm^{-2} sr^{-1} for the $T_{kin} = 20$ K fit.

The predicted integrated intensity of ^{12}CO 7–6 is very weak, varying strongly from 0.1 K km s^{-1} for the $T_{kin} = 20$ K solution to 1.9 K km s^{-1} for $T_{kin} = 100$ K.

Atomic carbon. Assuming the same density and temperature for carbon as for CO, we use the best fitting CO model to derive the [C I] 1–0 intensity, carbon column densities, and CO/C abundance ratios. The predicted CO/C abundance ratio is 0.15, again consistent with the optically thin LTE result. The predicted [C I] 2–1 integrated intensity is 6.1 K km s^{-1}.

As in NGC 4945, changing the temperature has a large effect on the [C I] 2–1 intensity. The $T_{kin} = 100$ K solution yields 111 K km s^{-1} and a higher CO/C abundance ratio of 1.67. Thus the [C I]2–1/[C I]1–0 line ratios changes from 0.04 to 0.74.

The corresponding carbon column densities for the two presented solutions are $N_C = 2.3 \times 10^{18}$ cm^{-2} and $N_C = 3.0 \times 10^{17}$ cm^{-2}, respectively. For the latter solution the column density is about a factor of 10 lower compared to the LTE carbon column density. The optically thin assumption for the LTE modelling is obviously not appropriate in the high temperature and low density scenario.

The total cooling intensity ratio of [C I]/CO varies from 2.1 to 2.8 for the presented solutions. Carbon is a stronger coolant than CO by a factor of 2–3.

5. Discussion

5.1. [C I] 1–0 luminosities

The [C I] 1–0 luminosities for the centers of the Seyfert galaxies NGC 4945 and Circinus are 91 and 67 K km s^{-1} kpc^2 (Fig. 4). To date, about 30 galactic nuclei have been studied in the 1–0 line of atomic carbon, most of which are presented in Gerin & Phillips (2000) and Israel & Baas (2002). The [C I] luminosity of a source is an important property since it gives the amount of energy emitted per time which is proportional to the number of emitting atoms, i.e. proportional to the [C I] column density in the limit of optically thin emission. The NANTEN2 38″ beam achieves ∼700 pc resolution in Circinus and NGC 4945 which both lie at ∼4 Mpc. To achieve the same spatial resolution for galaxies at ∼12 Mpc distance, e.g. for NGC 278, NGC 660, NGC 1068, NGC 3079 and NGC 7331 listed in Israel & Baas (2002), one would need an angular resolution of ∼13″, comparable to the 10″ JCMT beam at 492 GHz. The luminosities studied in these 7 sources thus all sample the innermost ∼700 pc. Area integrated [C I] luminosities are found to vary strongly between ∼1 and ∼160 K km s^{-1} kpc^2 in these 7 galaxies (Fig. 4) (Israel 2005; Israel & Baas 2002). Quiescent centers show modest luminosities $1 \leq L([\mathrm{C\,I}]) \leq 5$ K km s^{-1} kpc^2, while starburst nuclei in general show higher luminosities. The largest luminosities are found in the active nuclei of NGC 1068 and NGC 3079 which show 50 and 160 K km s^{-1} kpc^2 (Israel & Baas 2002). NGC 4945 and Circinus also fall in this category (Fig. 4).

5.2. [C I] 1–0/CO 4–3 line ratios

The [C I] 1–0/CO 4–3 ratio of integrated intensities is 1.2 in NGC 4945 and 2.8 in Circinus. For Circinus the ratio is larger than any ratios previously observed in other galactic nuclei or in the Milky Way. The [C I]1–0/CO 4–3 ratio is shown in Fig. 4 versus the area integrated [C I] luminosity. As also discussed in Israel & Baas (2002), we see no functional dependence. Galactic sources (not shown in this figure) would lie in the lower left corner. Israel (2005) studied 13 galactic nuclei and found that the [C I] 1–0 line is in general weaker than the CO 4–3 line, but not by much. Ratios vary over one order of magnitude between 0.1 in Maffei2 and 1.2 NGC 4826. Galactic star forming regions like W3 Main or the Carina clouds show much lower values, between about 0.1 and 0.5, which are consistent with emission from photon dominated regions (PDRs) (Kramer et al. 2004; Jakob et al. 2007; Kramer et al. 2007). Fixsen et al. (1999) find 0.22 in the Galactic center and 0.31 in the Inner Galaxy. The variation seen in the various Galactic and extragalactic sources appears to be intrinsic and not due to observations of different angular resolutions. This is because the frequencies of the two lines are very close and angular resolutions are therefore similar if the same telescope is used.

5.3. [C I] 1–0/ ^{13}CO 2–1 line ratios

The [C I] 1–0/ ^{13}CO 2–1 line ratios in NGC 4945 and Circinus are 5.51 and 8.57, respectively (Fig. 4). In NGC 4945, the observed ratio is consistent with results found in previous studies (Israel & Baas 2002; Gerin & Phillips 2000) ranging up to ratios of 5. For Circinus, the ratio is again higher than any previous measurement.

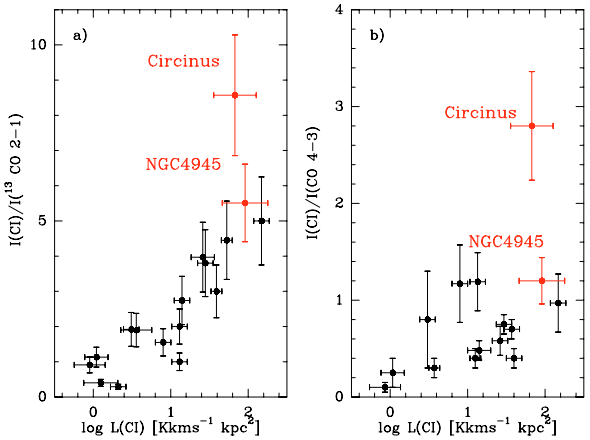

Fig. 4. a) [C I]1–0/^{13}CO 2–1 ratios versus L([C I]). **b)** [C I] 1–0/CO 4–3 ratios versus L([C I]). Black points are the results from Israel & Baas (2002) and red points are the ratios from this paper.

Two thirds of the sample of galaxies studied by Israel & Baas (2002) show [C I] 1–0/ ^{13}CO 2–1 line ratios well above unity. The sample consists of quiescent, star burst and active nuclei. The highest [C I] 1–0/ ^{13}CO 2–1 ratios are found in star burst and active nuclei, consistent with our observations. Gerin & Phillips (2000) find a similar result with two thirds of the galaxies in their sample exceeding a ratio of 2. High ratios can be qualitatively understood in low column density enviroments with mild UV radiation fields. In these regimes most CO will be dissociated and the gas-phase carbon will be neutral atomic (Israel & Baas 2002). This implies that dense, star forming molecular cloud cores are not the major emission source in galaxy centers.

In general the studied centers of external galaxies show stronger [C I] emission than one would expect from Galactic observations, which show typical ratios of 0.2–1.1 (Mookerjea et al. 2006). In Galactic sources high ratios are found in low gas column densities and medium UV radiation enviroments where ^{13}CO will be dissociated and atomic carbon remains neutral in the gas phase i.e. in translucent clouds and at cloud edges (Israel 2005). He concludes that the dominant emission from galaxy centers does not stem from PDRs.

Meijerink et al. (2007) studied irradiated dense gas in galaxy nuclei using a grid of XDR and PDR models. For the same density the predicted [C I] 1–0/ ^{13}CO 2–1 line ratios are significantly higher for the XDR- compared to PDR-models (Fig. 10 in Meijerink et al. 2007). We observed ratios of 61 and 95 in NGC 4945 and Circinus respectivly, on the erg-scale. These ratios can be explained by XDR-models at high densities $n(\mathrm{H_2}) = 2 \times 10^3$–$10^5$ cm^{-3}. PDR-models explain the observed ratios in low density regimes with $n(\mathrm{H_2}) = 2 \times 10^2$–$6 \times 10^2$ cm^{-3}. The high [C I] 1–0/ ^{13}CO 2–1 line ratios observed in NGC 4945 and Circinus may hint at a significant role of X-ray heating in these galaxy nuclei as our predicted densities of $n(\mathrm{H_2}) = 10^3$–10^4 cm^{-3} agree with the high-density XDR-models in Meijerink et al. (2007).

5.4. Total CO and [C I] cooling intensity

In all sources studied by Bayet et al. (2006) but NGC 6946, the CO cooling intensity exceeds that of atomic carbon. They find the [C I] to CO cooling ratio to vary between ∼0.3 for M83 to ∼2 for NGC 6946. NGC 4945 and Circinus show similarly high

values as the latter galaxy: in NGC 4945 this ratio is ∼1−2 and in Circinus we find ∼2−3. These values are around 2 orders of magnitude higher than the typical values found in Galactic star forming regions (Jakob et al. 2007; Kramer et al. 2007).

5.5. Shape of the CO cooling curve

The modeled CO cooling curve of NGC 4945 and Circinus peaks at $J = 4$. Observations of the higher lying CO lines i.e. the CO 6–5 and CO 7–6 lines will however be important to verify our model predictions and the importance of CO cooling relative to C.

The shape and maximum of the cooling curve of ^{12}CO has been studied in a number of nearby and high-z galaxies. Fixsen et al. (1999) find a peak at $J = 5$ in the central part of the Milky Way using FIRAS/COBE data and rotational transitions up to 8−7. Bayet et al. (2006) observed 13 nuclei in mid-J CO lines up to 7−6 and find that the peak of the cooling curves vary with nuclear activity. While normal nuclei exhibit peaks near $J_{up} = 4$ or 5, active nuclei show a peak near $J_{up} = 6$ or 7. NGC 253 was observed at APEX in CO upto $J_{up} = 7$ and shows a maximum at $J = 6$ (Güsten et al. 2006). On the other hand, studies of high redshift galaxies show cooling curves peaking as low as $J = 4$ for SMM 16359 (Weiß et al. 2005), as high as $J = 9$ in the case of the QSO APM 08279 (Weiss et al. 2007), and peaking at $J = 7$ for the very high redshift ($z = 6.4$) QSO J1148 (Walter et al. 2003).

5.6. Pressure of the molecular gas

A wide range of temperatures $T_{kin} = 25-150$ K and densities $n(H_2) = 5 \times 10^2 - 7 \times 10^5$ cm^{-3} has been found in similar studies of external nuclei, including ULIRGs, normal spirals, star burst galaxies, and interacting galaxies (e.g. Bayet et al. 2006; Israel & Baas 2002). In the irregular galaxy IC 10 rather high densities $n(H_2) \sim 10^6$ cm^{-3} and low temperatures of $T_{kin} = 25$ K are found while the molecular gas in the center of the spiral galaxy NGC 6946 is found to be less dense, $n(H_2) = 10^3$ cm^{-3}, but much hotter, $T_{kin} = 130$ K. Güsten et al. (2006) studied NGC 253 to obtain $n(H_2) = 10^{3.9}$ cm^{-3} and $T_{kin} = 60$ K while Bradford et al. (2003) investigated the same source and derived a higher $T_{kin} = 120$ K and density $n(H_2) = 4.5 \times 10^4$ cm^{-3}. Both studies used ^{12}CO 7–6 observations. However, the temperature/density degeneracy cannot be resolved. The solutions we present in our study of NGC 4945 and Circinus show densities and temperatures of $n(H_2) = 10^3 - 10^4$ cm^{-3} with a less well constrained temperature $T_{kin} = 20-100$ K; depending on the density, as discussed before.

5.7. [C I] 2–1/1–0 line ratio

The modeled [C I] 2–1/1–0 line ratios change from 0.07 to 0.75 in NGC 4945 and from 0.04 to 0.74 in Circinus for the presented escape probability solutions. Observed ratios vary from 0.48 in G333.0-0.4 (Tieftrunk et al. 2001) to 2.9 in W3 main for galactic and extragalactic sources (Kramer et al. 2004). For M82, Stutzki et al. (1998) found a ratio of 0.96. Bayet et al. (2006) observed ratios ranging between 1.2 (in NGC 253) to 3.2 (in IC 342). The [C I] 2–1/1–0 line ratio for the low temperature solution predicted for NGC 4945 and Circinus is significantly lower than previous results in the literature.

5.8. CO/C abundance ratio

Compared to an abundance ratio CO/C of 3−5 in NGC 253 (Bayet et al. 2004) and an average value of 2 in the nucleus of M83 (White et al. 1994; Israel & Baas 2001), NGC 4945 and Circinus have a higher fraction of atomic carbon in their nuclei which resembles the low CO/C abundance ratios found in Galactic translucent clouds. We find values of 0.23−0.64 in NGC 4945 and 0.15−1.67 in Circinus. Due to the degeneracy of $n(H_2)$, T the abundance ratios cannot be determined more accurately. In galactic molecular clouds values range between 0.16−100, low values are found in translucent clouds (Stark & van Dishoeck 1994) while massive star forming regions show high CO/C abundances (Mookerjea et al. 2006).

5.9. Future observations

Future observations of CO 7–6 and [C I] 2–1 will be important to better understand the the kinetic temperature and density to resolve their degeneracy, and for an understanding of the dominating heating mechanism i.e. X-ray or UV heating. We estimate detection of the [C I] 2–1 line with NANTEN2 within less than 10 min total observation time under average weather conditions. The CO 7−6 will be harder to detect, depending on the excitation conditions. At 810 GHz the 1 GHz bandwidth of the receiver translates into a velocity range of 370 km s^{-1}. We therefore plan to stack future observations to be able to cover the broad line widths of Circinus and NGC 4945.

Acknowledgements. We thank S. Curran for providing us with the SEST-data for Circinus, R. Mauersberger and G. Rydberg for SEST-data for NGC 4945, and R.Güsten and S. Philipp for the APEX-data of NGC 253. The NANTEN2 project (southern submillimeter observatory consisting of a 4-m telescope) is based on a mutual agreement between Nagoya University and The University of Chile and includes member universities from six countries, Australia, Republic of Chile, Federal Republic of Germany, Japan, Republic of Korea, and Swiss Confederation. We acknowledge that this project could be realized by financial contributions of many Japanese donators and companies. This work is financially supported in part by a Grant-in-Aid for Scientific Research from the Ministry of Education, Culture, Sports, Science and Technology of Japan (No.15071203) and from JSPS (No. 14102003 and No.18684003), and by the JSPS core-to-core program (No.17004). This work is also financially supported in part by the grant SFB 494 of the Deutsche Forschungsgemeinschaft, the Ministerium für Innovation, Wissenschaft, Forschung und Technologie des Landes Nordrhein-Westfalen and through special grants of the Universität zu Köln and Universität Bonn. L.B. and J.M. acknowledge support from the Chilean Center for Astrophysics FONDAP 15010003.

References

Aalto, S., Booth, R. S., Black, J. H., & Johansson, L. E. B. 1995, A&A, 300, 369
Ables, J. G., Forster, J. R., Manchester, R. N., et al. 1987, MNRAS, 226, 157
Bayet, E., Gerin, M., Phillips, T., & Contursi, A. 2004, A&A, 427, 45
Bayet, E., Gerin, M., Phillips, T. G., & Contursi, A. 2006, A&A, 460, 467
Bradford, C. M., Nikola, T., Stacey, G. J., et al. 2003, ApJ, 586, 891
Brock, D., Joy, M., Lester, D. F., Harvey, P. M., & Ellis, H. B. J. 1988, ApJ, 329, 208
Cunningham, M. R., & Whiteoak, J. B. 2005, MNRAS, 364, 37
Curran, S. J., Johansson, L. E. B., Rydbeck, G., & Booth, R. S. 1998, A&A, 338, 863
Curran, S. J., Johansson, L. E. B., Bergman, P., Heikkilä, A., & Aalto, S. 2001a, A&A, 367, 457
Curran, S. J., Polatidis, A. G., Aalto, S., & Booth, R. S. 2001b, A&A, 368, 824
Dahlem, M., Golla, G., Whiteoak, J. B., et al. 1993, A&A, 270, 29
de Vaucouleurs, G., de Vaucouleurs, A., Corwin, H. J., et al. 1991, Third reference catalogue of bright galaxies (New York: Springer-Verlag)
Dos Santos, P. M., & Lépine, J. R. D. 1979, Nature, 278, 34
Elmouttie, M., Krause, M., Haynes, R. F., & Jones, K. L. 1998, MNRAS, 300, 1119
Farquhar, P. R. A., Millar, T. J., & Herbst, E. 1994, in American Institute of Physics Conference Series, Molecules and Grains in Space, ed. I. Nenner, 312, 135

Fixsen, D. J., Bennett, C. L., & Mather, J. C. 1999, ApJ, 526, 207
Freeman, K. C., Karlsson, B., Lynga, G., et al. 1977, A&A, 55, 445
Frerking, M. A., Langer, W. D., & Wilson, R. W. 1982, ApJ, 262, 590
Frerking, M. A., Keene, J., Blake, G. A., & Phillips, T. G. 1989, ApJ, 344, 311
Fullmer, L., & Londsdale, C. J. 1989, Cataloged galaxies and quasars observed in the IRAS survey, JPL D, Pasadena: Jet Propulsion Laboratory, Version 2
García-Burillo, S., Martín-Pintado, J., Fuente, A., & Neri, R. 2001, ApJ, 563, L27
Gardner, F. F., & Whiteoak, J. B. 1982, MNRAS, 201, 13
Gerin, M., & Phillips, T. G. 2000, ApJ, 537, 644
Ghosh, S. K., Bisht, R. S., Iyengar, K. V. K., et al. 1992, ApJ, 391, 111
Greenhill, L. J., Herrnstein, J. R., Ellingsen, S. P., et al. 1998, in BAAS, 1332
Güsten, R., Philipp, S. D., Weiß, A., & Klein, B. 2006, A&A, 454, L115
Henkel, C., Whiteoak, J. B., & Mauersberger, R. 1994, A&A, 284, 17
Israel, F. P. 2005, Ap&SS, 295, 171
Israel, F. P., & Baas, F. 2001, A&A, 371, 433
Israel, F. P., & Baas, F. 2002, A&A, 383, 82
Iwasawa, K., Koyama, K., Awaki, H., et al. 1993, ApJ, 409, 155
Jakob, H., Kramer, C., Simon, R., et al. 2007, A&A, 461, 999
Johansson, L. E. B., Aalto, S., Booth, R. S., & Rydbeck, G. 1991, in Dynamics of Disc Galaxies, ed. B. Sundelius, 249
Kramer, C., Jakob, H., Mookerjea, B., et al. 2004, A&A, 424, 887
Kramer, C., Mookerjea, B., Bayet, E., et al. 2005, A&A, 441, 961
Kramer, C., Cubick, M., Röllig, M., et al. 2007, A&A, submitted
Lonsdale, C. J., & Helou, G. 1985, Cataloged galaxies and quasars observed in the IRAS survey, Pasadena: Jet Propulsion Laboratory (JPL)
Maiolino, R., Salvati, M., Bassani, L., et al. 1998, A&A, 338, 781
Mauersberger, R., Henkel, C., Whiteoak, J. B., Chin, Y.-N., & Tieftrunk, A. R. 1996, A&A, 309
Meijerink, R., Spaans, M., & Israel, F. P. 2007, A&A, 461, 793
Mookerjea, B., Kramer, C., Röllig, M., & Masur, M. 2006, A&A, 456, 235
Moorwood, A. F. M., & Oliva, E. 1994, ApJ, 429, 602
Mueller Sánchez, F., Davies, R. I., Eisenhauer, F., et al. 2006, A&A, 454, 481
Ott, M. 1995, Ph.D. Thesis, Univ. Bonn
Ott, M., Whiteoak, J. B., Henkel, C., & Wielebinski, R. 2001, A&A, 372, 463
Papadopoulos, P. P., & Greve, T. R. 2004, ApJ, 615, L29
Rekola, R., Richer, M. G., McCall, M. L., et al. 2005, MNRAS, 361, 330
Risacher, C., Vassilev, V., Monje, R., et al. 2006, A&A, 454, L17
Sanders, D. B., & Mirabel, I. F. 1996, ARA&A, 34, 749
Schinke, R., Engel, V., Buck, U., Meyer, H., & Diercksen, G. 1985, ApJ, 299, 939
Simon, R., Graf, U., Kramer, C., Stutzki, J., & Onishi, T. 2007, Technical Report: Beam efficieny measurements at NANTEN
Stark, R., & van Dishoeck, E. F. 1994, A&A, 286, L43
Strong, A. W., & Mattox, J. R. 1996, A&A, 308, L21
Strong, A. W., Bloemen, J. B. G. M., Dame, T. M., et al. 1988, A&A, 207, 1
Stutzki, J., & Winnewisser, G. 1985, A&A, 144, 13
Stutzki, J., Bensch, F., Heithausen, A., Ossenkopf, V., & Zielinsky, M. 1998, A&A, 336, 697
Tieftrunk, A., Jacobs, K., Martin, C., et al. 2001, A&A, 23, 23
Usero, A., García-Burillo, S., Martín-Pintado, J., Fuente, A., & Neri, R. 2006, A&A, 448, 457
Walter, F., Bertoldi, F., Carilli, C., et al. 2003, Nature, 424, 406
Wang, M., Henkel, C., Chin, Y.-N., et al. 2004, A&A, 422, 883
Weiß, A., Downes, D., Walter, F., & Henkel, C. 2005, A&A, 440, L45
Weiss, A., Downes, D., Neri, R., et al. 2007, A&A, 467, 955
White, G. J., Ellison, B., Claude, S., Dent, W. R. F., & Matheson, D. N. 1994, A&A, 284, L23
Whiteoak, J. B., Dahlem, M., Wielebinski, R., & Harnett, J. I. 1990, A&A, 231, 25
Wilson, A. S., Shopbell, P. L., Simpson, C., et al. 2000, AJ, 120, 1325